journal

J. Am. Ceram. Soc., 97 [4] 1264–1268 (2014)
DOI: 10.1111/jace.12747

A New Ferroelectric Phase of $YMnO_3$ Induced by Oxygen-Vacancy Ordering

Qinghua Zhang, Sandong Guo, Binghui Ge, Peng Chen, Yuan Yao, Lijuan Wang, Lin Gu, Yanguo Wang, Xiaofeng Duan, Changqing Jin, Banggui Liu, and Richeng Yu†

Beijing National Laboratory for Condensed Matter Physics, Institute of Physics, Chinese Academy of Sciences, Beijing 100190, China

Manganese oxides are good candidates of strongly correlated electron materials due to the uniqueness of electronic structure of manganese and the mobility of oxygen among lattice sites under external impacts. Here, we used electron beam as the excitation source to explore the structural evolution of $YMnO_3$ and identified a new phase under the radiation of electron beam in the transmission electron microscope. Analyses of the electron energy-loss spectra reveal that this phase originates from ordered oxygen vacancy. We applied the first principles calculation to pick out the optimized stable structure with a lower polarization, and verified its correctness by electron diffraction and image simulations. Analyses of density of states indicate that weak Y–O covalence is favorable for the existence of ferroelectricity, supporting the electrostatic nature of ferroelectricity in the $YMnO_3$.

I. Introduction

The abundant magnetic ferroelectric materials are good candidates for exploring the physical nature of the interaction between spins and charges. As a prototypical improper ferroelectric, the hexagonal $RMnO_3$ (R = Sc, Y, Ho to Lu) has attracted tremendous attentions because of the coexistence of antiferromagnetism (AFM) and ferroelectricity (FE), which is very appropriate for investigating the electron–lattice interaction in multiferroics.[1–4] The multiferroicity is characterized with the coexistence of the spontaneous magnetization and polarization that can be switched by an applied electric and magnetic field, respectively, and indicates promising fascinating applications in memory devices.[5,6] Generally, the magnetism and FE are exclusive to each other in perovskite-structure oxides because of the d^0-ness mechanism proposed by Hill.[7] The hexagonal $YMnO_3$ is a rare and valuable exceptional subject of multiferroicity due to its large size mismatch of ionic radius and layered structure. Compared to other multiferroics, such as $BiFeO_3$, one of the hottest subjects in multiferroics, $YMnO_3$ exhibits strong and intrinsic coupling between the ferroelectric and the magnetic orderings, which displays ferroelectric ordering far above room temperature (>900 K) and antiferromagnetic ordering at low temperature (~80 K).[8] To design new materials with enhanced magnetoelectric coupling, the understanding about intrinsic mechanisms of the multiferroicity is indispensable. However, a very basic issue about the exact origin of the improper FE of $YMnO_3$ is not clear yet, at least in inconformity among different groups.

Originally, its unusual electronic structure had been suspected to the origin of the FE by density-functional theory calculation.[9,10] However, Van Aken *et al.*[1] defied it basing on X-ray refinement and the first principles calculation, and then concluded that the electrostatic and size effect are responsible for the FE of $YMnO_3$. Subsequently, Cho *et al.*[11] proposed the Y d^0-ness mechanism and regarded that the Y d^0-ness with rehybridization is the driving force for the FE using the polarization-dependent X-ray spectroscopy. Very recently, Liu *et al.*[12] prepared the samples annealed at different temperatures which show the structural transformation from the orthorhombic to the hexagonal, carried out the analyses of X-ray refinement and X-ray absorption near-edge spectra and ascribed that the FE is caused by the charge transfer from the $Y–O_T$ bond to the $Mn–O_T$ bond. As a result, mechanisms for the origin of the FE in $YMnO_3$ have been ambiguous and confusing so far.

Here, we apply the transmission electron microscopy (TEM) and the density-functional theory (DFT) calculation to investigate the new structure evolved from $YMnO_3$ under the radiation of electron beam. With the use of selected-area electron diffraction (SAED), high-resolution transmission electron microscopy (HRTEM), and electron energy-loss spectroscopy (EELS), the new ferroelectric structures involving with ordered oxygen vacancies are proposed. The DFT calculation was applied to testify possible structure models and pick out the optimized stable structure with a lower polarization, which was verified by electron diffraction and image simulations. To understand its FE with the lower polarization, we performed the density of states (DOS) calculation, indicating that weak Y–O covalence is favorable for the existence of FE in $YMnO_3$.

II. Experimental Procedure

Polycrystalline $YMnO_3$ samples were synthesized by a conventional solid-state reaction method. A stoichiometric mixture of Y_2O_3 and Mn_2O_3 powders was well ground and calcined twice in air at 1200°C for 24 h. The X-ray diffraction was performed on a Philips X'Pert Propowder diffractometer (PANalytical B.V., Almelo, The Netherlands) ($CuK_{\alpha 1}$ λ = 1.5406 Å) with a scan step of 0.017° and confirmed the purity of the samples. The thin samples for TEM observations were prepared by crushing the grains in an agate mortar filled with alcohol, then dispersing the resulting fine fragments suspended in alcohol on holey carbon films supported by copper grids. The TEM observations were carried out on a FEI F20 electron microscope (FEI, Eindhoven, The Netherlands) with field-emission gun and a JEM-2010 electron microscope (JEOL Ltd., Tokyo, Japan) with LaB_6 fragment, which are both operated at 200 keV.

III. Results and Discussion

At high temperature above ~900 K, $YMnO_3$ crystallizes in paraelectric state with space group $P6_3/mmc$ (Ref. [4]), and its lattice parameters are a = 3.63 and c = 11.35 Å. As shown in Fig. 1(a), the MnO_5 bipyramids are connected by

X. Tan—contributing editor

Manuscript No. 33266. Received May 29, 2013; approved November 3, 2013.
†Author to whom correspondence should be addressed. e-mail: rcyu@aphy.iphy.ac.cn

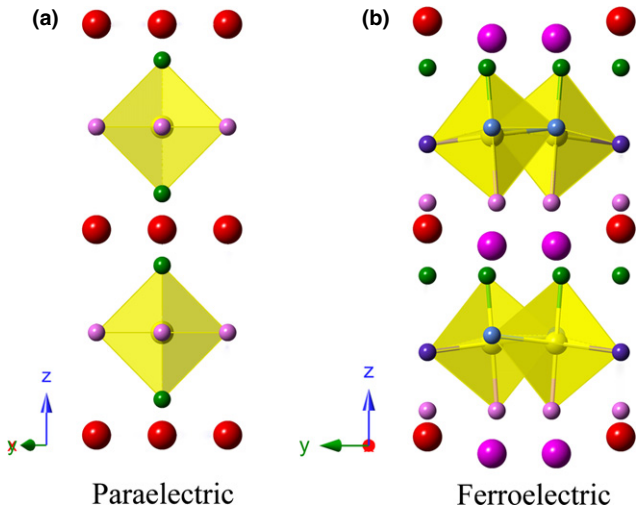

Fig. 1. The structure models for the paraelectric (a) and primary ferroelectric (b) $YMnO_3$. The red and pink spheres with the big radius represent Y ions. The yellow spheres represent Mn ions, the smallest spheres represent nonequivalent oxygen ions, and the yellow bipyramids label out the MnO_5.

sharing corner in *ab* plane, all Y ions are equivalent and locate at the positions with the same *c* value, and MnO_5 bipyramids and Y ions are arranged alternately layer by layer along *c* axis. Because of its centrosymmetric unit cell, there is no electric polarization in the paraelelctric state. In contrast, in its ferroelectric unit cell with space group $P6_3cm$ shown in Fig. 1(b), Y ions decompose into two nonequivalent types (denoted by red and pink spheres); a wave-like arrangement of Y ions appears along the view direction of *a* axis, which demonstrates that $YMnO_3$ is in the ferroelectric state. In our study, we observed that the period of ferroelectric lattice transforms to a modulated paraelectric period under the radiation of electron beam at room temperature.

Figure 2 shows the SAED patterns containing the new phase. Under the radiation with an intense electron beam (~150 A/cm^2) for 2 min, the extra diffraction spots marked by the white frames gradually begin to appear, indicating the formation of an ordered structure. Figures 2(a) and (b) are the SAED patterns obtained from the mixed region of the primary ferroelectric and new phases of $YMnO_3$, recorded along [010] and [1-10] directions, respectively (the subscript *p* represents the primary ferroelectric phase). The diffraction spots marked by the white arrows in Fig. 2(a) arise from the primary ferroelectric phase, corresponding to the tripling of the paraelectric unit cell. It should be noted that we always get the mixed diffraction patterns because that the new phase only evolves from the thinnest region of the sample and cannot be separated from the nearby ferroelectric region in the electron diffraction. After systematic tilting experiments in TEM, we confirm that the diffraction spots are corresponding to the $2a \times 2a \times c$ periodicity of the paraelectric unit cell.

The mixed nature of electron-diffraction patterns presented above were further verified after investigating a HRTEM image containing the new phase recorded on conventional TEM films with large field of view. Figure 2(c) is an HRTEM image including the primary ferroelectric $YMnO_3$ phase, showing the origin of the new phase. The image presented here is Fourier filtered to minimize the effect of the contrast noise. Three regions can be identified by their corresponding FFTs. We find out that the new phase only resides at the edge of the specimen. Twice periodicity of the paraelectric phase can be identified obviously in this direction, comparing to the triple periodicity in the ferroelectric phase. Combining the evidences from the SAED patterns and HRTEM images above, we can make a conclusion that there is a new phase coexisting with the primary ferroelectric phase.

To find out the origin of this new structure, we have carried out EELS studies. The EELS relates to the interaction of the fast electrons with the sample and reflects discrete transitions between atomic energy levels, allowing both compositional analysis and the determination of degree of

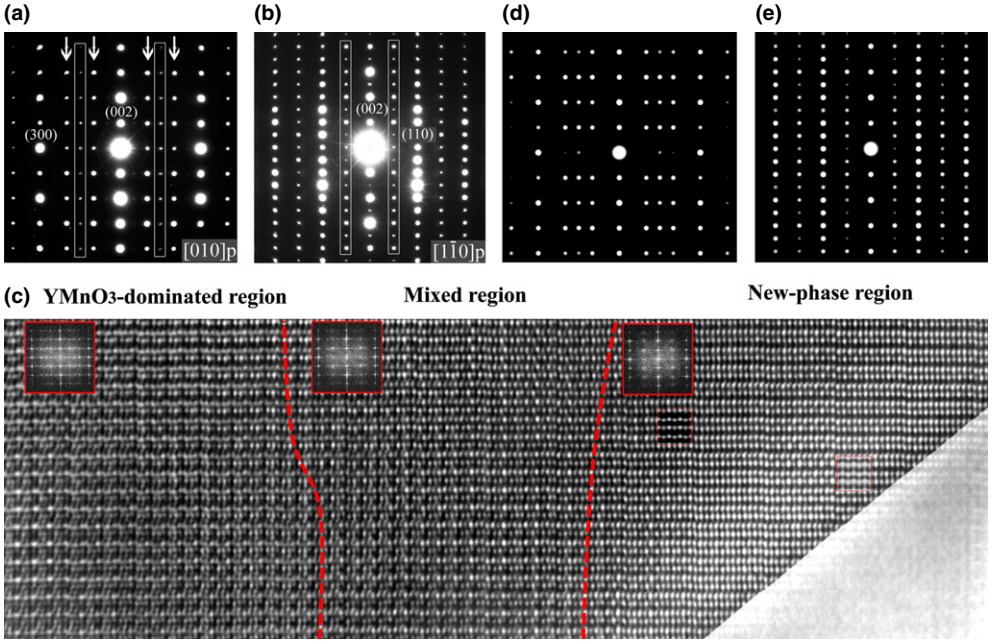

Fig. 2. The selected-area electron-diffraction (SAED) patterns and high-resolution transmission electron microscopy (HREM) images of the new phase and the simulations. (a)–(b) The SAED patterns along the [010] and [1-10] zone axes in the coordinate system of the primary ferroelectric phase, respectively. (c) is an HRTEM image including the primary ferroelectric $YMnO_3$ phase. Three regions can be identified by their corresponding FFTs. Two red broken lines indicate the boundaries. Two simulated images (indicated by small rectangles) with thicknesses of 6.3 nm (on the right side) and 8.8 nm (on the left side) are superposed on the new phase region to match the experimental image, where the contrast is adjusted according to the background of the experimental image. The simulated SAED patterns (d), (e) correspond to the [010]p and [1-10]p experimental patterns in (a) and (b), respectively.

bonding hybridization. Particularly, its near-edge structure contains valuable information about the nearest-neighbored bonding (O 2*p* with the cationic *d*-orbital) and the hybridization with the *sp* band. Hence, we also recorded EELS spectra from both the primary ferroelectric phase and the subsequent modulated phase after electron beam radiation. There are obvious changes in the ELNES of O *K* and Mn $L_{2,3}$ edges as shown in Figs. 3(a) and (b), respectively. Three characteristic peaks marked by *a*, *b*, and *c* can be clearly distinguished, where peak *a* is related to the hybridization between O and Mn ions, *b* and *c* reflects the hybridization between O and Y ions, and the two spectra are normalized to have the same intensity of peak *a*. The relative intensity of peak *b* of the new phase is considerably lower than that of the primary ferroelectric phase. According to the previous studies,[13,14] oxygen vacancies have an important influence on the relative intensity of peaks *a* and *b* of yttrium oxide. Thus, the decrease in the peak *b* demonstrates the appearance of the oxygen vacancies in nonstoichiometric $YMnO_{3-\delta}$. Meanwhile, the measured L_3/L_2 ratio of Mn $L_{2,3}$ edges shows an increase from 2.77 to 3.12 after the appearance of the new phase, corresponding to the decreasing of the valence state of Mn ions. We also performed the quantification of the EELS spectra and obtained the O–Mn atomic ratio of 2.96 and 2.74 for the stoichiometric $YMnO_3$ and the new phase, respectively. This result indicates that there are about two oxygen vacancies in the $2a \times 2a \times c$ supercell of the paraelectric phase.

On the basis of the analyses above, we have constructed structure models with ordered oxygen vacancies and two possible models (O1 and O2) are proposed, as shown in Figs. 4(a) and (b). The position of the first oxygen vacancy is at the same upper left part of the supercell above the brown MnO_4 in the two models. The second oxygen vacancy resides under the brown MnO_4 in O1 rather than above the brown MnO_4 in O2. With systematic symmetry analysis, we obtain the space groups $P31m$ and $P6_3mc$ for O1 and O2, respectively. It should be noted that because the lattice vectors of the paraelectric and ferroelectric unit cells have a rotation angle of 90° between each other in the *ab* plane, space group $P6_3mc$ is equivalent to $P6_3cm$ in the primary ferroelectric unit cell. That is to say, O2 preserves the same symmetry as $YMnO_3$.

To determine the possible ground state, we performed the first principles calculation using the full-potential linearized augmented plane waves method within the DFT[15] using the Vienna Ab-initio Simulation Package.[16] The generalized gradient approximation (GGA)[17] is used for the exchange-correlation potential, and the internal position parameters are optimized using the A-type AFM arrangement[1] of Mn moment with a force standard of 2 mRy/a.u.. The energy calculations indicate that O2 with the space group of $P6_3mc$ is the possible ground state by saving 1.3 eV per unit cell compared with O1. In addition, we have verified this new structure with the simulations of the SAED patterns and HRTEM image using the optimized O2. Figures 2(d) and (e)

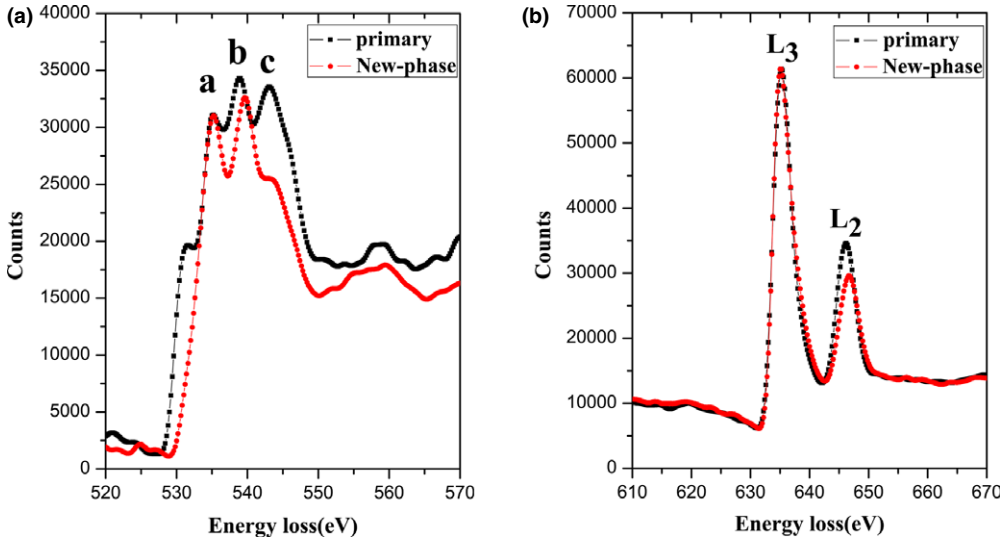

Fig. 3. The electron energy-loss spectroscopy spectra of O *K* edge and Mn $L_{2,3}$ edges. (a) is the ELNES of O K edge; (b) is the ELNES of Mn $L_{2,3}$ edges. Peak *a* is related to the hybridization between O and Mn ions, *b* and *c* reflect the hybridization between O and Y ions.

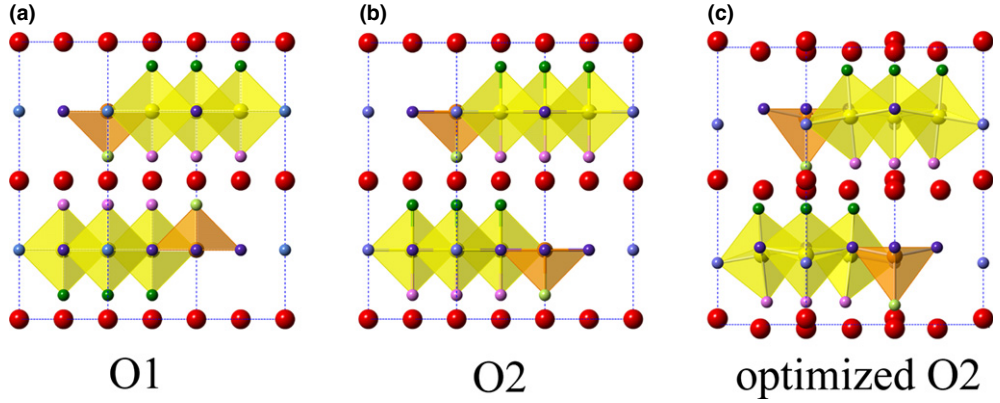

Fig. 4. The structural models for O1 (a), O2 (b), and the optimized O2 (c). The red spheres represent R ions, the polyhedra represent MnO_5 and MnO_4, and the oxygen atoms position at the corners of the polyhedra.

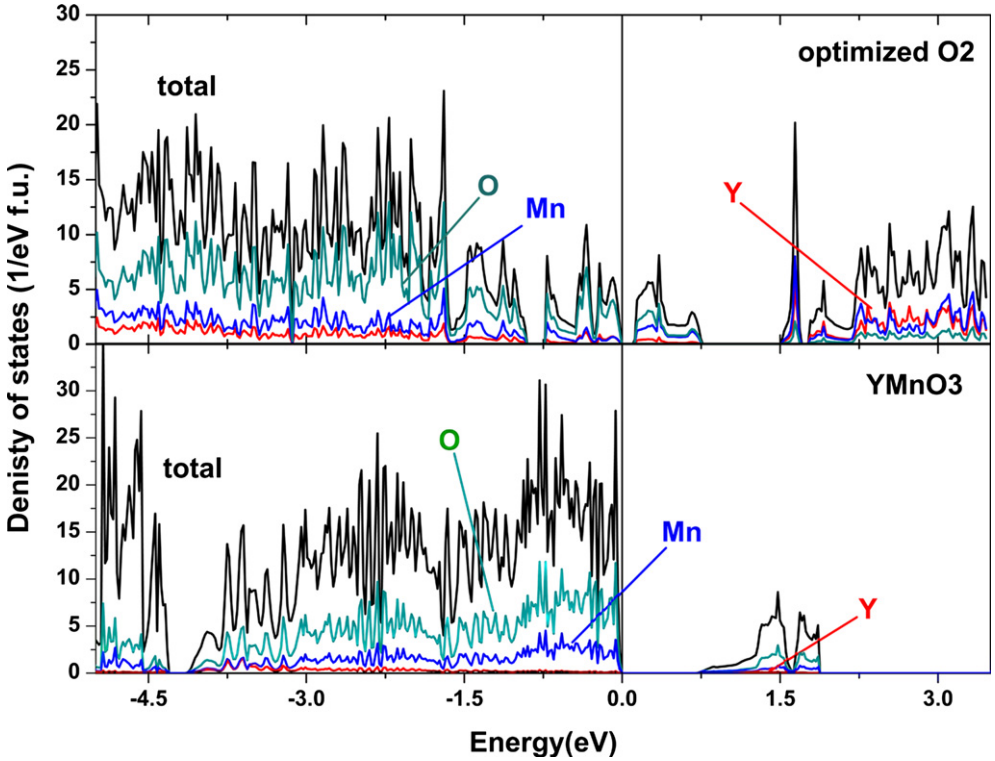

Fig. 5. Calculated total density of states and partial density of states of optimized O2 and $YMnO_3$. Valence bands are composed mainly of O-2*p* and Mn-3*d* orbital. The difference of the electronic structures is mainly manifested at the density of states of Y ions.

show the simulated SAED patterns and two simulated HRTEM images by multislice method[18] under the conditions of 6.3 and 8.8 nm in thickness, and −184 nm in defocus are inserted in the new phase region of Fig. 2(c). The simulated results show a good agreement with the experimental ones.

The spontaneous polarizations were also calculated within the GGA (the LDA + U gives almost the same results) with a plane wave basis sets and projector augmented wave pseudopotentials, which is performed by using the Berry-phase formalism.[19,20] To testify the validity of the algorithm, we first calculated the spontaneous polarization for the primary ferroelectric $YMnO_3$ structure and obtained a ferroelectric polarization of 6.7 $\mu C/cm^2$, which is close to the measured value (5.2 $\mu C/cm^2$)[21] and the theoretical value (6.2 $\mu C/cm^2$).[1] Then, we calculate the spontaneous polarization for the optimized O2 and obtain a value of 4.6 $\mu C/cm^2$, which is smaller than that of the primary ferroelectric $YMnO_3$. These results demonstrate that the new structure is also ferroelectric, but its spontaneous polarization is reduced due to the existence of the ordered oxygen vacancies.

To elucidate the origin of the FE in this new phase in perspective of electronic structure, we calculate its DOS. Figure 5 displays the total DOS of the primary ferroelectric $YMnO_3$ and new phases, respectively. Compared with $YMnO_3$, the total DOS of the new phase shows different positions of valence band relative to the Fermi level, and a narrower gap that can be ascribed to the appearance of the ordering of oxygen vacancy (acts as a defect state). The bands above the Fermi level also move toward lower energies. Compared with the DOS of $YMnO_3$, there is an obvious increase above the Fermi level in the DOS of Y ions in the optimized O2, which indicates a stronger covalence between O and Y ions. Recent theoretical study (Ref. [22]) about $YMnO_3$ and $InMnO_3$ also revealed that the absence of covalence favors the ferroelectric phase. On the basis of the decreased polarization in the optimized O2, we suggest that the weak Y–O covalence is favorable for the existence of FE in the $YMnO_3$.

The total energy calculation also reproduced the atomic displacements relative to the positions of their paraelectric equivalents as shown in Fig. 4(c). The buckling of Y ions and tilting of MnO_5 occur in the crystal structure of the optimized O2. We compared the displacements between the up-down Y layers and the tilting of MnO_5 between $YMnO_3$ and O2, which change from 47 to 41 pm and from 3.9° to 4.6°, respectively. Both the two changes suppress the polarization. It should be noted that so far we have not obtained bulk material with ordered oxygen vacancies, so we lack of the experimentally obtained ferroelectric properties of the new phase. At present, we have to resort to the DFT calculation. The work of preparing the oxygen-deficient sample is now undergoing.

IV. Conclusions

We applied TEM and DFT calculation to the investigation of the new ferroelectric phase evolved from $YMnO_3$, which originates from oxygen-vacancy ordering induced by electron beam irradiation. We proposed the structure model O2 and verified its correctness by DFT calculations and TEM simulations. Our results demonstrate that the smaller displacements of Y ions and stronger Y–O covalence are responsible for the lower polarization, indicating that weak Y–O covalence is favorable for the existence of FE in the $YMnO_3$.

Acknowledgments

This work was financially supported by the State Key Development Program for Basic Research of China (grant nos. 2012CB932302 and 2010CB934202), the National Natural Science Foundation of China (grant nos. 11174336 and 11174359).

References

[1]B. B. Van Aken, T. T. M. Palstra, A. Filippetti, and N. A. Spaldin, "The Origin of Ferroelectricity in Magnetoelectric $YMnO_3$," *Nat. Mater.*, **3**, 164–70 (2004).

[2]S. W. Cheong and M. Mostovoy, "Multiferroics: A Magnetic Twist for Ferroelectricity," *Nat. Mater.*, **6**, 13–20 (2007).
[3]W. Eerenstein, N. D. Mathur, and J. F. Scott, "Multiferroic and Magnetoelectric Materials," *Nature*, **442**, 759–65 (2006).
[4]T. Katsufuji, M. Masaki, A. Machida, M. Moritomo, K. Kato, E. Nishibori, M. Takata, M. Sakata, K. Ohoyama, K. Kitazawa, and H. Takagi, "Crystal Structure and Magnetic Properties of Hexagonal $RMnO_3$ (R=Y, Lu, and Sc) and the Effect of Doping," *Phys. Rev. B*, **66**, 134434 (2002).
[5]N. Hur, S. Park, P. A. Sharma, J. S. Ahn, S. Guha, and S. W. Cheong, "Electric Polarization Reversal and Memory in a Multiferroic Material Induced by Magnetic Fields," *Nature (London)*, **429**, 392–5 (2004).
[6]T. Kimura, T. Goto, H. Shintani, K. Ishizaka, T. Arima, and Y. Tokura, "Magnetic Control of Ferroelectric Polarization," *Nature*, **426**, 55–8 (2003).
[7]N. A. Hill, "Why Are There So Few Magnetic Ferroelectrics?" *J. Phys. Chem. B, 2000*, **104**, 6694–709 (2000).
[8]Z. J. Huang, Y. Cao, Y. Y. Sun, Y. Y. Xue, and C. W. Chu, "Coupling Between the Ferroelectric and Antiferromagnetic Orders in $YMnO_3$," *Phys. Rev. B*, **56**, 2623–6 (1997).
[9]M. Qian, J. Dong, and Q. Zheng, "Electronic Structure of the Ferroelectromagnet $YMnO_3$," *Phys. Lett. A*, **270**, 96–101 (2000).
[10]A. Filippetti and N. A. Hill, "Coexistence of Magnetism and Ferroelectricity in Perovskites," *Phys. Rev. B*, **65**, 195120 (2002).
[11]D.-Y. Cho, J.-Y. Kim, B.-G. Park, K.-J. Rho, J.-H. Park, H.-J. Noh, B. J. Kim, S.-J. Oh, H.-M. Park, J.-S. Ahn, H. Ishibashi, S.-W. Cheong, J. H. Lee, P. Murugavel, T. W. Noh, A. Tanaka, and T. Jo, "Ferroelectricity Driven by Y d^0-Ness with Rehybridization in $YMnO_3$," *Phys. Rev. Lett.*, **98**, 217601 (2007).
[12]S.-H. Liu, J.-C.-A. Huang, X. D. Qi, W.-J. Lin, Y.-J. Siao, C.-R. Lin, J.-M. Chen, M.-T. Tang, Y.-H. Lee, and J.-C. Lee, "Structural Transformation and Charge Transfer Induced Ferroelectricity and Magnetism in Annealed $YMnO_3$," *AIP Adv.*, **1**, 032173 (2011).
[13]F. Jollet, C. Noguera, M. Gautier, N. Thromat, and J.-P. Duraud, "Influence of Oxygen Vacancies on the Electronic Structure of Yttrium Oxide," *J. Am. Ceram. Soc.*, **74**, 358–64 (1991).
[14]A. Travlos, N. Boukos, G. Apostolopoulos, and A. Dimoulas, "Oxygen Vacancy Ordering in Epitaxial Layers of Yttrium Oxide on Si (001)," *Appl. Phys. Lett.*, **82**, 4053–5 (2003).
[15]P. Hohenberg and W. Kohn, "Inhomogeneous Electron Gas," *Phys. Rev. B*, **136**, B864–71 (1964).
[16]G. Kresse and D. Joubert, "From Ultrasoft Pseudopotentials to the Projector Augmented-Wave Method," *Phys. Rev. B*, **59**, 1758–75 (1999).
[17]J. P. Perdew, K. Burke, and M. Ernzerhof, "Generalized Gradient Approximation Made Simple," *Phys. Rev. Lett.*, **77**, 3865–8 (1996).
[18]J. M. Cowley and A. F. Moodie, "The Scattering of Electrons by Atoms and Crystals," *Acta Cryst.*, **10**, 609–19 (1957).
[19]R. D. King-Smith, and D. Vanderbilt, "Theory of Polarization of Crystalline Solids," *Phys. Rev. B*, **47**, 1651–4 (1993).
[20]D. Vanderbilt and R. D. King-Smith, "Electric Polarization as a Bulk Quantity and its Relation to Surface Charge," *Phys. Rev. B*, **48**, 4442–55 (1993).
[21]N. Fujimura, T. Ishida, T. Yoshimura, and T. Ito, "Epitaxially Grown $YMnO_3$ Film: New Candidate for Nonvolatile Memory Devices," *Appl. Phys. Lett.*, **69**, 1011–3 (1996).
[22]Y. Kumagai, A. A. Belik, M. Lilienblum, N. Leo, M. Fiebig, and N. A. Spaldin, "Observation of Persistent Centrosymmetricity in the Hexagonal Manganite Family," *Phys. Rev. B*, **85**, 174422 (2012). □